GEOPHYSICAL RESEARCH LETTERS, VOL. 35, L15105, doi:10.1029/2008GL034493, 2008

Ambient solar wind's effect on ICME transit times

A. W. Case,[1] H. E. Spence,[1] M. J. Owens,[1] P. Riley,[2] and D. Odstrcil[3]

Received 28 April 2008; revised 13 June 2008; accepted 27 June 2008; published 8 August 2008.

[1] Most empirical and numerical models of Interplanetary Coronal Mass Ejection (ICME) propagation use the initial CME velocity as their primary, if not only, observational input. These models generally predict a wide spread of 1 AU transit times for ICMEs with the same initial velocity. We use a 3D coupled MHD model of the corona and heliosphere to determine the ambient solar wind's effect on the propagation of ICMEs from 30 solar radii to 1 AU. We quantitatively characterize this deceleration by the velocity of the upstream ambient solar wind. The effects of varying solar wind parameters on the ICME transit time are quantified and can explain the observed spread in transit times for ICMEs of the same initial velocity. We develop an adjustment formula that can be used in conjunction with other models to reduce the spread in predicted transit times of Earth-directed ICMEs. **Citation:** Case, A. W., H. E. Spence, M. J. Owens, P. Riley, and D. Odstrcil (2008), Ambient solar wind's effect on ICME transit times, *Geophys. Res. Lett.*, *35*, L15105, doi:10.1029/2008GL034493.

1. Background and Introduction

[2] Interplanetary Coronal Mass Ejections (ICMEs) are huge eruptions of solar plasma and magnetic field that are episodically ejected into the heliosphere and are a major cause of intense space weather observed at Earth [*Gosling*, 1993]. Undesirable consequences of ICMEs range from geomagnetic storms to energetic particles, which are accelerated in interplanetary space [*Feynman and Gabriel*, 2000]. With better knowledge of ICME properties, particularly their arrival time, precautionary measures could be taken to mitigate the effects on space hardware and human explorers.

[3] By correlating CME speeds near the Sun with ICME speeds observed at 1 AU, it has been shown that fast ICMEs are decelerated towards the ambient solar wind velocity [*Gopalswamy et al.*, 2000]. This deceleration has been modeled in a variety of ways. *Vršnak and Gopalswamy* [2002] and *Cargill* [2004] modeled it analytically as an effective drag force that acts on the ICME after it is ejected from the Sun. *Gopalswamy et al.* [2000] used two-point measurements (coronagraph and *in situ* observations at L1) to construct an empirical model that assumes a constant deceleration over the entire trajectory to Earth, and *Gopalswamy et al.* [2001] allowed the deceleration to cease at some radial distance from the Sun. *Cargill and Schmidt* [2002] used 2.5-D MHD codes to simulate ICME propagation.

[4] Recent studies have shown that the solar wind is important in determining the transit time of ICMEs. Using a combination of solar wind data from upstream and downstream of ICMEs, *Vršnak and Žic* [2007] observed that the solar wind can greatly influence the transit time of an ICME from the sun to 1 AU. *Manoharan* [2006] observed ICMEs near Earth with interplanetary scintillation techniques and arrived at the same conclusions.

[5] Previous attempts to model ICMEs have been unable to predict the transit time to within better than ±10 hours [e.g., *Gopalswamy et al.*, 2000, 2001; *Manoharan*, 2006]. This indicates that the initial speed of the CME is an insufficient predictor of transit time. *Owens and Cargill* [2004] found that the upstream ambient solar wind velocity was not a major contributor to the spread in transit times of ICMEs, but recently *Schwenn et al.* [2005] suggested and *Vršnak and Žic* [2007] showed that variations in the Ambient Solar Wind (ASW) could cause this wide spread in transit time.

[6] Global MHD codes allow us to visualize and model the heliosphere in ways that are otherwise not possible through remote or *in situ* observations. We use this ability to better understand the factors influencing the trajectory of ICMEs. In this study, we use a 3D magnetohydrodynamic (MHD) model of the heliosphere to simulate the propagation of ICMEs out to 1 AU. The ICMEs are ejected directly toward Earth from 30 R_S (the inner boundary of the heliospheric model) into a wide variety of ASWs. The goals of this paper are to: (1) quantify how the ASW affects the trajectory of the ICME as it moves toward Earth, and (2) to use these results to better predict the transit times of ICMEs.

2. Inserting and Tracking ICMEs in Global MHD Model

[7] In order to simulate the propagation of an ICME, we use a pair of coupled 3-D MHD models. The innermost model is "MHD Around a Sphere" (MAS, §2.1) and is driven by observed photospheric magnetograms. Output at MAS's outer boundary is coupled (§2.3) to the inner boundary (30 R_S) of the Enlil model of the heliosphere (§2.2). This model then solves the MHD equations on a Sun-centered spherical grid out to 2 AU. At the boundary of the two models, an overpressured density cloud is inserted as a proxy for the driver of the ICME.

2.1. The MAS Model of the Corona

[8] The global corona is modeled by the Magnetohydrodynamics Around a Sphere (MAS) 3D MHD code [*Linker et al.*, 1999; *Mikic et al.*, 1999]. Photospheric magnetic field observations provide the boundary conditions, from which initial conditions are derived by a potential field solution to

[1]Center for Space Physics, Boston University, Boston, Massachusetts, USA.
[2]Science Applications International Corporation, San Diego, California, USA.
[3]Space Weather Prediction Center, NOAA, Boulder, Colorado, USA.

0094-8276/08/2008GL034493$05.00

the photospheric radial field, a uniform boundary density, and a Parker-type solar wind outflow. The time-dependent polytropic MHD equations, with finite resistivity and viscosity, are then solved in a spherical geometry between 1 and 30 R_S. The solution is allowed to relax to a dynamic steady state. *Linker and Mikić* [1997] provide a more detailed description of the initial and boundary conditions, and *Lionello et al.* [1999] describe the details of the algorithm. In this paper, we use the polytropic version of MAS with a mesh of 60, 70, and 64 grid cells in the radial (r), meridional (θ), and azimuthal (ϕ) directions, respectively. The mesh is non-uniform in r and θ, with more resolution at lower altitudes and surrounding the heliographic equator.

[9] The polytropic version of MAS yields nearly isothermal solutions, which qualitatively reproduce many coronal properties. However, the plasma velocity does not reproduce the large speed variations that are observed between the fast and slow wind. To provide more realistic lower boundary conditions for the heliospheric MHD model (§2.2), the plasma velocity from the coronal model is replaced with an empirically derived velocity that is based on the modeled MHD magnetic field configuration [*Riley et al.*, 2001], in a similar manner to the Wang-Sheeley-Arge model [*Arge et al.*, 2004].

2.2. The Enlil Model of the Heliosphere

[10] The heliosphere is modeled using the "Enlil" 3D ideal MHD code developed at the NOAA Space Weather Prediction Center (SWPC) [*Odstrcil*, 2003, and references therein]. The computational domain covers 30 R_S to 2 AU, and $-60°$ to $+60°$ in solar latitude. The lower boundary conditions for the Enlil model are provided by a coronal solution from the MAS model. The heliospheric solution is allowed to relax to steady state. We use a version of the Enlil code for computational efficiency that uses 256, 30, and 90 grid cells in the radial, meridional, and azimuthal directions, respectively.

2.3. Coupled Models With ICMEs

[11] The "CORHEL" model couples the MAS MHD model of the corona (§2.1) with the Enlil MHD model of the heliosphere (§2.2). In this study, MAS is driven with magnetograms from the National Solar Observatory and is coupled to Enlil at 30 R_S. See *Odstrcil et al.* [2004a] and *Luhmann et al.* [2004] for more detail. CORHEL has been shown to match the bulk properties of the ambient solar wind very well [*Owens et al.*, 2008].

[12] At the code-coupling boundary an overpressured cloud is inserted to simulate an ICME. The cloud is four times more dense and has the same temperature as the ASW and is inserted as a spherical pulse with a diameter of the user-specified width [*Odstrcil et al.*, 2004b]. In contrast to other MHD studies [e.g., *Cargill*, 2004], it should be noted that the inserted ICME does not contain an intrinsic magnetic field: whereas magnetic pressure may be dominant in reality, plasma pressure is dominant here. The ICME's initial radial velocity, direction, and angular width are specified by the user, typically on the basis of "cone model" fits to coronagraph observations [e.g., *Odstrcil et al.*, 2004b]. In this study, all ICMEs are launched directly toward Earth with an angular width of 45°.

3. Solar Wind's Effect on ICME Trajectory

[13] After an ICME is inserted into the model, we track its center of mass as the ICME propagates toward Earth. At the time of insertion, in order to characterize the ASW, we average the radial velocity of the solar wind that will be intercepted by the ICME's trajectory. We average from 30 R_S to the first parcel of solar wind that will reach Earth in the same amount of time as the ICME at its initial velocity. We use this metric to characterize the solar wind as we expect speed to only slightly increase with distance from the sun, in contrast to density which decreases dramatically with radial distance. We also anticipate that the ASW velocity should affect transit time of ICMEs, as predicted by a simple drag deceleration model [*Cargill*, 2004].

[14] In the MHD model, we ejected five ICMEs with the same structure, location and diameter, but different initial velocity each into four different ambient solar winds. Four specific consecutive Carrington Rotations, CRs 1955–1958, were chosen because, collectively, they represent the full range of ASW speeds that an ICME might encounter. These CRs were chosen because CORHEL predictions match the L1-observed solar wind structure particularly well during this period. All of the ICMEs were inserted at a radial velocity of at least 700 km/s, in order to be initially faster than the ASW. Though slower ICMEs are also affected by the ASW, they were not used in this study due to the difficulty in characterizing the downstream ASW that would serve to accelerate such ICMEs. The initial speeds were 700, 1000, 1300, 1600, and 1900 km/s. The transit times of these 20 ICMEs are shown in Figure 1 as a function of initial velocity. The transit times have been adjusted to 6 R_S by assuming that they travel at their initial velocity inside of 30 R_S.

[15] A sub-set of ICMEs from the list of 91 unique CME-ICME connections from *Schwenn et al.* [2005] is also shown in Figure 1. We selected only those CMEs that were 360° halos and for which an expansion speed had been specified. The transit times for ICMEs from *Schwenn et al.* [2005] are plotted against their measured expansion speeds, which was found to be a good proxy for the true radial velocity. These transit times are from the time of first appearance in the LASCO C2 coronagraph, which images the solar corona in white light from 1.5 to 6 R_S [*Brueckner et al.*, 1995], until the time of shock arrival at 1 AU. *Schwenn et al.* [2005] fit their observations with a logarithmic function and found that the standard deviation of their data was 14 hours. Solid black lines are plotted in Figure 1 at 1σ above and below the best-fit function. We define the spread in observed transit times (Schwenn dT) to be 2σ = 28 hours.

[16] All of the simulated ICMEs experienced deceleration during their transit to 1 AU. Though the cause of this deceleration will not be investigated in this work, we suspect that it is caused by the MHD equivalent of a drag force that tends to equalize the speeds of the ICME and the ambient solar wind. Simulated ICMEs that were inserted into the ambient winds from CRs 1955 and 1957 encountered an average V_{SW} that was relatively slow and resulted

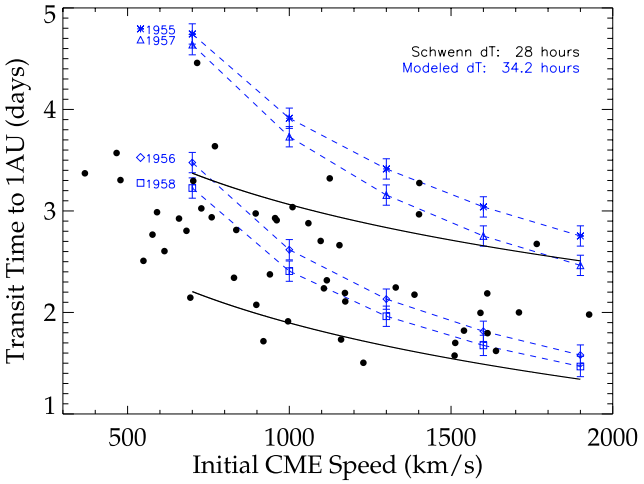

Figure 1. Transit times (from 6 R_S to 1 AU) as a function of the initial speed for modeled ICMEs are shown as points connected by dashed lines, and are grouped according to the Carrington rotation in which they were injected. Filled circles are CME-ICME pairs found by *Schwenn et al.* [2005] to be 360° halos and their transit times are from their first appearance in LASCO to 1 AU. The standard deviation of these points from a best-fit logarithmic function was 14 hours, and solid black lines indicate $\pm 1\sigma$ from this function. 'Schwenn dT' is defined as 2σ. 'Modeled dT' is defined as the average of the time difference between the maximum and minimum arrival times at each initial ICME velocity. As discussed in Section 5, the model does not predict all absolute transit times, but the spread in modeled transit times is sufficient to explain the spread in the observed points.

in much more deceleration, and hence a longer transit time. The opposite was true for CRs 1956 and 1958. We calculate the spread in modeled transit times (Modeled dT) by averaging the maximum difference in transit times at each initial velocity. We find this spread to be 34.2 hours. As discussed in Section 5, the model does not accurately predict the absolute transit time of ICMEs. However, these representative extreme cases show that the solar wind has a profound influence (more than a full day) on the transit time of ICMEs, and can explain the observed spread in transit times for CMEs that start with the same initial velocity [*Schwenn et al.*, 2005].

4. Adjustment Formula

[17] Using the model results, we now develop a formula that can be used to better predict the transit time of ICMEs. It is intended that this adjustment be used with models of ICME transit time that do not explicitly account for the effect of ambient solar wind [e.g., *Gopalswamy et al.*, 2000, 2001; *Michaek et al.*, 2004; *Kim et al.*, 2007].

[18] We sorted our modeled ICMEs according to their initial velocity and plotted them in the top plot of Figure 2. A quadratic best fit of the form: $T = A(V_{SW})^2 + B(V_{SW}) + C$ is plotted as a dotted line for each set of ICMEs. A quadratic function was chosen since it was found to fit the data much better than a simple linear function. Furthermore, a quadratic form is consistent with the expected drag force [*Cargill*, 2004]. We fit a quadratic function to the entire set of modeled points and constructed a formula (shown in the bottom plot of Figure 2) that provides an adjustment to the transit time about a typical solar wind speed of 440 km/s. Thus, our adjustment formula is as follows:

$$T_{ADJ} = A(\Delta V)^2 + B(\Delta V) \quad (1)$$

where $\Delta V = V_{SW} - 440$ km/s. We find the best fit to be with $A = 8.5 \times 10^{-6} \frac{(\text{days})\text{s}^2}{\text{km}^2}$ and $B = -0.0047 \frac{(\text{days})\text{s}}{\text{km}}$. This fit is shown as the solid line in Figure 2.

5. Discussion and Conclusions

[19] Observations show that when an ICME interacts with the ambient solar wind (ASW), its velocity tends to approach that of the ASW [*Gopalswamy et al.*, 2000]. It has been suggested [*Schwenn et al.*, 2005] that variations in the solar wind conditions and its interaction with an ICME could cause the observed spread in transit times for ICMEs with similar initial velocities. We have used 3D MHD simulations to confirm this hypothesis and further quantified the effects of the ASW, in order to better predict the transit time of ICMEs.

[20] We inserted ICMEs into a wide range of ambient solar wind conditions in a 3D MHD model and tracked their centers of mass out to 1 AU. For CMEs with similar initial velocities, changing only the ambient solar wind conditions

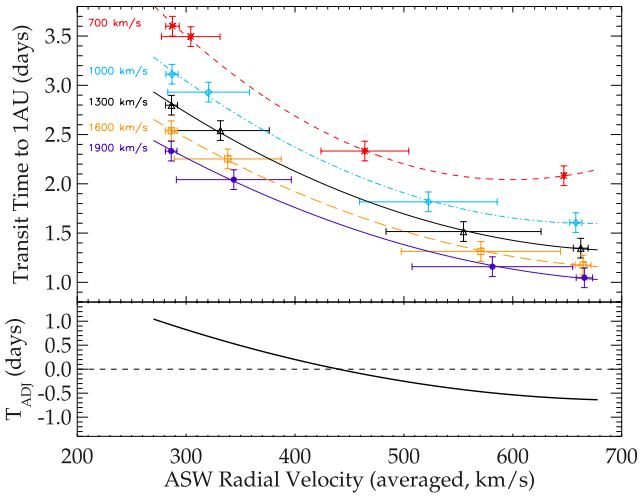

Figure 2. (top) Modeled transit times as a function of the radial velocity of the ambient solar wind. Points are grouped according to the initial speed of the ICME and are shown along with a least-squares quadratic fit for each group. Horizontal error bars indicate the standard deviation of the solar wind speed that each ICME encounters. Vertical error bars indicate a standard ±0.1 day uncertainty in the determination of each ICMEs arrival time at 1 AU due to the temporal spacing of our model snapshots. (bottom) Calculated adjustment formula as a function of the ASW radial velocity.

encountered by the ICME can explain the spread in transit times observed by other studies [*Schwenn et al.*, 2005].

[21] The transit times of the CMEs show a clear dependence on the ambient solar wind conditions (Figure 2). We assumed that the transit time is a quadratic function of the average velocity of the ambient solar wind that the ICME will encounter on its way to Earth. We plotted the transit time of CMEs with the same initial velocity against the mean ASW velocity upstream of the ICME. We found that the ASW causes a difference in transit time of up to a day. As expected, the modeled absolute transit times (especially for slower CMEs) do not agree with observations. This could result from *Schwenn et al.* [2005] using white light images near the sun, but shock arrival times at 1 AU. The shock could precede the density enhancements by up to a day. [e.g., *Owens and Cargill*, 2004]. Despite these differences in absolute transit times, the spread in transit times is similar.

[22] Equation (1) shows the formula developed, which factors in the ambient solar wind's effect on the transit time of ICMEs. This equation should allow a quick, more accurate prediction of an ICME's arrival time at Earth, provided an initial estimate of transit time (presumably from a model with initial CME velocity as its input) and some knowledge of the solar wind upstream of the ICME. Knowledge of the upstream solar wind could come from observations (e.g., Heliospheric Imager on STEREO), or from ambient solar wind models such as the Wang-Sheeley-Arge (WSA) model, or CORHEL.

[23] While the effects of the ambient solar wind are sufficient to explain the observed spread in transit times, we cannot be certain that this is the cause. In particular, we recognize that ICMEs not launched directly toward Earth could appear to arrive at different times due to an impact with the flank rather than the nose of the ICME. If ICMEs have concave-outward structures, then the ''nose'' of the ejection will arrive at 1-AU before the flanks. However, this picture is further complicated by the fact that ICMEs have typical angular widths of about $\sim$60–90 degrees, and hence span large variations in ambient solar wind speed. This ambient solar wind speed gradient can result in significant distortion of the ejecta, meaning the measured arrival time will depend strongly on the point of interception [*Schmidt and Cargill*, 2001; *Owens*, 2006]. The contribution of this 'shape' effect to transit time uncertainty could be important and certainly warrants future investigation.

[24] It is not clear how accurately plane-of-sky velocities from halo events can be converted into true radial velocities. Conversion from plane-of-sky to radial speed may have a significant contribution to the spread in transit times observed for CMEs with the same apparent initial speed. The model in this paper has been constructed using true radial velocities from modeled ICMEs, and so the use of CME velocities that are not the true radial velocity could impart some error to our correction formula.

[25] Despite the aforementioned contributions to transit time uncertainty, our models show that the upstream ASW velocity alone is sufficient to explain the entire observed spread in transit times for CMEs of similar initial speeds. This effect should be taken into consideration when predicting the transit times of ICMEs to 1 AU.

[26] **Acknowledgments.** This work was supported by the LRO/CRaTER project under contract NASA NNG05EB92C. This work was also partially supported by CISM, an NSF Science and Technology Center funded under agreement ATM-0120950.

References

Arge, C. N., J. G. Luhmann, D. Odstrcil, C. J. Schrijver, and Y. Li (2004), Stream structure and coronal sources of the solar wind during the May 12th, 1997 CME, *J. Atmos. Sol. Terr. Phys.*, *66*, 1295–1309, doi:10.1016/j.jastp.2004.03.018.

Brueckner, G. E., et al. (1995), The large angle spectroscopic coronagraph (LASCO), *Sol. Phys.*, *162*, 357–402, doi:10.1007/BF00733434.

Cargill, P. J. (2004), On the aerodynamic drag force acting on interplanetary coronal mass ejections, *Sol. Phys.*, *221*, 135–149, doi:10.1023/B:SOLA.0000033366.10725.a2.

Cargill, P. J., and J. M. Schmidt (2002), Modelling interplanetary cmes using magnetohydrodynamic simulations, *Ann. Geophys.*, *20*, 879–890.

Feynman, J., and S. B. Gabriel (2000), On space weather consequences and predictions, *J. Geophys. Res.*, *105*(A5), 10,543–10,564, doi:1999JA000141.

Gopalswamy, N., L. Lara, R. P. Lepping, M. L. Kaiser, D. Berdichevsky, and O. C. St. Cyr (2000), Interplanetary acceleration of coronal mass ejections, *Geophys. Res. Lett.*, *27*(2), 145–148.

Gopalswamy, N., A. Lara, S. Yashiro, M. L. Kaiser, and R. A. Howard (2001), Predicting the 1-AU arrival times of coronal mass ejections, *J. Geophys. Res.*, *106*(A12), 29,207–29,217.

Gosling, J. T. (1993), The solar flare myth, *J. Geophys. Res.*, *98*(A11), 18,937–18,950, doi:10.1029/93JA01896.

Kim, K.-H., Y.-J. Moon, and K.-S. Cho (2007), Prediction of the 1-AU arrival times of CME-associated interplanetary shocks: Evaluation of an empirical interplanetary shock propagation model, *J. Geophys. Res.*, *112*, A05104, doi:10.1029/2006JA011904.

Linker, J. A., and Z. Mikić (1997), Extending coronal models to earth orbit, in *Coronal Mass Ejections, Geophys. Monogr. Ser.*, vol. 99, edited by N. Crooker, J. Joselyn, and J. Feynman, pp. 269–278, AGU, Washington, D. C.

Linker, J. A., Z. Mikić, D. A. Biesecker, R. J. Forsyth, S. E. Gibson, A. J. Lazarus, A. Lecinski, P. Riley, A. Szabo, and B. J. Thompson (1999), Magnetohydrodynamic modeling of the solar corona during Whole Sun Month, *J. Geophys. Res.*, *104*(A5), 9809–9830.

Lionello, R., Z. Mikić, and J. A. Linker (1999), Stability of algorithms for waves with large flows, *J. Comput. Phys.*, *152*, 346–358.

Luhmann, J. G., S. C. Soloman, J. A. Linker, J. G. Lyon, Z. Mikic, D. Odstrcil, W. Wang, and M. Wiltberger (2004), Coupled model simulation of a Sun-to-Earth space weather event, *J. Atmos. Sol. Terr. Phys.*, *66*, 1243–1256.

Manoharan, P. K. (2006), Evolution of coronal mass ejections in the inner heliosphere: A study using white-light and scintillation images, *Sol. Phys.*, *235*, 345–368.

Michaek, G., N. Gopalswamy, A. Lara, and P. K. Manoharan (2004), Arrival time of halo coronal mass ejections in the vicinity of the Earth, *Astron. Astrophys.*, *423*, 729–736, doi:10.1051/0004-6361:20047184.

Mikic, Z., J. A. Linker, D. D. Schnack, R. Lionello, and A. Tarditi (1999), Magnetohydrodynamic modeling of the global solar corona, *Phys. Plasmas*, *6*, 2217.

Odstrcil, D. (2003), Modeling 3-D solar wind structures, *Adv. Space Res.*, *32*, 497–506.

Odstrcil, D., V. Pizzo, J. A. Linker, P. Riley, R. Lionello, and Z. Mikic (2004a), Initial coupling of coronal and heliospheric numerical magnetohydrodynamic codes, *J. Atmos. Sol. Terr. Phys.*, *66*, 1311–1320.

Odstrcil, D., P. Riley, and X. P. Zhao (2004b), Numerical simulation of the 12 May 1997 interplanetary CME event, *J. Geophys. Res.*, *109*, A02116, doi:10.1029/2003JA010135.

Owens, M. J. (2006), Magnetic cloud distortion resulting from propagation through a structured solar wind: Models and observations, *J. Geophys. Res.*, *111*, A12109, doi:10.1029/2006JA011903.

Owens, M., and P. Cargill (2004), Predictions of the arrival time of coronal mass ejections at 1 AU: An analysis of the causes of errors, *Ann. Geophys.*, *22*, 661–671.

Owens, M. J., H. E. Spence, S. L. McGregor, W. J. Hughes, J. M. Quinn, C. N. Arge, P. Riley, J. A. Linker, and D. Odstrcil (2008), Metrics for solar wind prediction models: Comparison of empirical, hybrid and physics-based schemes with 8 years of L1 observations, *Space Weather*, doi:10.1029/2007SW000380, in press.

Riley, P., J. A. Linker, and Z. Mikic (2001), An empirically-driven global MHD model of the solar corona and inner heliosphere, *J. Geophys. Res.*, *106*(A8), 15,889–15,902.

Schmidt, J. M., and P. J. Cargill (2001), Magnetic cloud evolution in a two-speed solar wind, *J. Geophys. Res.*, *106*(A5), 8283–8290, doi:10.1029/2000JA900171.

Schwenn, R., A. Dal Lago, E. Huttunen, and W. D. Gonzalez (2005), The association of coronal mass ejections with their effects near the Earth, *Ann. Geophys.*, *23*, 1033–1059.

Vršnak, B., and N. Gopalswamy (2002), Influence of the aerodynamic drag on the motion of interplanetary ejecta, *J. Geophys. Res.*, *107*(A2), 1019, doi:10.1029/2001JA000120.

Vršnak, B., and T. Žic (2007), Transit times of interplanetary coronal mass ejections and the solar wind speed, *Astron. Astrophys.*, *472*, 937–943, doi:0.1051/0004-6361:20077499.

A. W. Case, M. J. Owens, and H. E. Spence, Center for Space Physics, Boston University, 725 Commonwealth Avenue, Boston, MA 02215, USA. (tonycase@gmail.com)

D. Odstrcil, Space Weather Prediction Center, NOAA, 325 Broadway, Boulder, CO 80305, USA.

P. Riley, Science Applications International Corporation, 10260 Campus Point Drive MS-M3W, San Diego, CA 92121-1578, USA.